

RESEARCH ARTICLE

10.1002/2014JD021672

This article is a companion to *Ahn et al.* [2014] doi:10.1002/2013JD020188.

Key Points:

- Globally, OMI and AERONET SSA agree for 46% (69%) of matchups within 0.03(0.05)
- Robust agreement at AOD > 0.4 and UV-AI > 1.0 for smoke then dust and urban aerosols
- Revision in surface/aerosol properties can enhance the accuracy of OMI retrieval

Correspondence to:

H. Jethva,
hiren.t.jethva@nasa.gov

Citation:

Jethva, H., O. Torres, and C. Ahn (2014), Global assessment of OMI aerosol single-scattering albedo using ground-based AERONET inversion, *J. Geophys. Res. Atmos.*, 119, 9020–9040, doi:10.1002/2014JD021672.

Received 20 FEB 2014

Accepted 18 JUN 2014

Accepted article online 24 JUN 2014

Published online 28 JUL 2014

Global assessment of OMI aerosol single-scattering albedo using ground-based AERONET inversion

Hiren Jethva^{1,2}, Omar Torres², and Changwoo Ahn³

¹Universities Space Research Association, Columbia, Maryland, USA, ²Laboratory of Atmospheric Chemistry and Dynamics, Code 614, NASA Goddard Space Flight Center, Greenbelt, Maryland, USA, ³Science Systems and Applications Inc., Lanham, Maryland, USA

Abstract We compare the aerosol single-scattering albedo (SSA) retrieved by the near-UV two-channel algorithm (OMAERUV) applied to the Aura/Ozone Monitoring Instrument (OMI) measurements with an equivalent inversion made by the ground-based Aerosol Robotic Network (AERONET). A recent upgrade of the OMAERUV algorithm incorporates a modified carbonaceous aerosol model, a Cloud-Aerosol Lidar with Orthogonal Polarization-based aerosol height climatology, and a robust aerosol-type identification. This paper is the first comprehensive effort to globally compare the OMI-retrieved SSA with that of AERONET using all available sites spanning the regions of biomass burning, dust, and urban pollution. An analysis of the colocated retrievals over 269 sites reveals that about 46% (69%) of OMI-AERONET matchups agree within the absolute difference of ± 0.03 (± 0.05) for all aerosol types. The comparison improves to 52% (77%) when only “smoke” and “dust” aerosol types were identified by the OMAERUV algorithm. Regionally, the agreement between the two inversions was robust over the biomass burning sites of South America, Sahel, Indian subcontinent, and oceanic/coastal sites followed by a reasonable agreement over Northeast Asia. Over the desert regions, OMI tends to retrieve higher SSA, particularly over the Arabian Peninsula. Globally, the OMI-AERONET matchups agree mostly within ± 0.03 for the aerosol optical depth (440 nm) and UV-aerosol index larger than 0.4 and 1.0, respectively. Possible sources of uncertainty in the OMI retrieval can be the subpixel cloud contamination, assumptions of the surface albedo, and spectral aerosol absorption. We expect further refinement in the OMAERUV algorithm which stands uniquely in characterizing aerosol absorption from space.

1. Introduction

Remote sensing of aerosols from satellite-based sensors has become an essential tool to detect, monitor, and quantify the aerosol optical and size properties over the globe on a daily basis. This is an important requirement for reducing the uncertainty in aerosol-related impact on the radiation balance (direct and semidirect effects) and cloud microphysics (indirect effect), which currently are not well characterized in the global estimates of radiative forcing [*Intergovernmental Panel on Climate Change, 2007*]. The fundamental aerosol parameters which primarily determine the strength and sign of the radiative forcing are the aerosol optical depth (AOD) and single-scattering albedo (SSA). While the columnar AOD represents the total extinction (scattering and absorption) as a result of interactions with solar radiation, SSA describes the relative strength of scattering to the total extinction. For instance, an SSA of 0.9 indicates that 90% (10%) of the total extinction of solar light is caused by scattering (absorption) effects. The importance of these two parameters lies in a fact that both together, more importantly SSA, determine the magnitude and sign of the aerosol radiative forcing. For example, a decrease in SSA from 0.9 to 0.8 can often change the sign of radiative forcing from negative (cooling) to positive (warming) that also depends on the albedo of the underlying surface and the altitude of the aerosols [*Hansen et al., 1997*]. Thus, an accurate estimate of both of these quantities is a prime requirement for arriving at a reliable prognosis on the net effect of atmospheric aerosols associated with the anthropogenic as well as natural activities.

Since its launch in July 2004, the Ozone Monitoring Instrument (OMI) on board NASA's Aura satellite has measured reflected radiation from Earth in the 270–500 nm wavelength range of the spectrum globally on a daily basis. With a cross-track swath of about 2600 km at ground level, OMI scans the entire Earth in 14 to 15 orbits with a nadir ground pixel spatial resolution of $13 \times 24 \text{ km}^2$. Satellite observations at 354 and 388 nm made by OMI are used to derive UV aerosol index (UV-AI) as well as the AOD and SSA using a near-UV

algorithm (OMAERUV) that takes the advantage of the well-known sensitivity to the aerosol absorption in the UV spectral region [Torres *et al.*, 1998]. While a general description of the OMI/OMAERUV algorithm is presented in Torres *et al.* [2007], the recent algorithmic upgrades are documented in Torres *et al.* [2013]. In addition to this, Lee *et al.* [2007] also developed a method that uses ground-based AOD and space-based spectral reflectance measurements synergistically to retrieve SSA at the visible wavelengths.

Recently, the two-channel OMI/OMAERUV algorithm has gone through an important revision in which three major modifications were incorporated. The algorithm uses a set of new carbonaceous aerosol models that account for the presence of organics in the carbonaceous aerosols [Jethva and Torres, 2011]. Previously, black carbon was assumed to be the sole component which was represented by the wavelength-independent imaginary index. Now the new carbonaceous aerosol models are incorporated with a wavelength-dependent imaginary index in the near-UV region as a proxy for the presence of organics [Kirchstetter *et al.*, 2004]. In the revised algorithm, the identification of aerosol type has been improved by taking an advantage of the Atmospheric Infrared Sounder (AIRS) carbon monoxide (CO) observations in conjunction with OMI UV-AI. Initially, the assumption on the aerosol layer height was tied to the Goddard Chemistry Aerosol Radiation and Transport model simulations. The new algorithm uses the aerosol height climatology derived from Cloud-Aerosol Lidar with Orthogonal Polarization (CALIOP) lidar-based measurements of the vertical profiles of aerosol for the carbonaceous and dust aerosols [Torres *et al.*, 2013].

In previous papers [Torres *et al.*, 2007; Ahn *et al.*, 2008; Jethva and Torres, 2011], the OMI-retrieved AOD and SSA were assessed against those of AERONET over a few selected sites located in the smoke- and dust-dominated environments. Since the inception of the OMAERUV algorithm and several upgrades thereafter, a global assessment of OMI aerosol product has been lacking. Recently, a validation analysis of the OMAERUV AOD product using AERONET measurements has been carried out by Ahn *et al.* [2014]. In the present paper, we have compared the reprocessed OMAERUV retrievals of SSA with those from the Aerosol Robotic Network (AERONET). AERONET is a global ground-based network of Sun photometer that routinely derives the columnar AOD and SSA in the visible and near-IR wavelength bands as well as particle size information over hundreds of sites spread over the major biomass burning, dust, and urban/industrial regions of the world [Holben *et al.*, 1998]. A further description on the AERONET data set is presented in section 2. Note that unlike in the direct Sun photometer-satellite AOD comparison in which the surface-based measurement is regarded as a ground truth value, we emphasize here that a comparison between AERONET and OMAERUV SSA measurements does not constitute a validation analysis since both measuring techniques are based on inversion algorithms that rely on assumptions. The resulting level of agreement can only be interpreted as a measure of consistency (or lack thereof) in the measurement of the same physical parameter by fundamentally different remote sensing approaches.

Section 2 describes the satellite and ground-based data sets assessed in this analysis along with the collocation methodology. A regional representation of sites, possible aerosol types over these locations, and the results of OMI versus AERONET comparison for the biomass burning, dust, and urban pollution regions are presented in section 3. The possible sources of uncertainty in both inversion products and a sensitivity analysis of the OMAERUV retrievals for selected case studies are presented in section 4. The paper is concluded in section 5.

2. Data Set

2.1. OMAERUV Aerosol Retrieval

The entire record of OMI observations (October 2004 to present) has been reprocessed with the new OMAERUV algorithm (PGEVersion V1.4.2) to derive AOD and SSA at 388 nm. The retrieved parameters are also reported at 354 nm and 500 nm. The data set is available in the HDF-EOS 5 format and can be obtained at no cost from NASA Goddard Earth Sciences (GES)-Data and Information Services Center (DISC) server at <http://daac.gsfc.nasa.gov/>. Since the recent upgrade has been documented in detail in the work of Torres *et al.* [2013] and Ahn *et al.* [2014], readers are referred to these two papers for in-depth description of the OMAERUV algorithm. We use the OMAERUV Level 2 Collection 003 (V1.4.2) aerosol product that was processed in March 2012. The OMAERUV algorithm assigns quality flag to each pixel which carries information on the quality of the retrieval. We use aerosol retrieval with quality flag 0 which is considered to be the best in accuracy.

Each cross-track OMI swath consists of 60 pixels, also termed as rows. Since mid-2007, OMI observations have been affected by a likely external obstruction that perturbs both the measured solar flux and Earth radiance. This obstruction affecting the quality of radiance at all wavelengths for a particular viewing direction is referred to as "row anomaly" since the viewing geometry is associated with the row numbers on the charge-coupled device detectors. The row anomaly issue was detected first time in mid-2007 with a couple of rows which over the period of operation expanded to other rows in 2008 and later. At present, about half of the total 60 rows across the track are identified and flagged as row anomaly affected positions for which no physical retrievals are being performed. The details about this issue can be found at <http://www.knmi.nl/omi/research/product/rowanomaly-background.php>. This has significantly affected the sampling during post-2008 OMI measurements, where about half of the OMI swath is blanketed by row anomaly flags. As a result, the availability of the number of retrievals over a particular station is reduced starting in 2009 compared to earlier OMI measurements. Consequently, the number of OMI-AERONET matchups is also expected to be reduced during row anomaly affected period.

2.2. AERONET

The Aerosol Robotic Network (AERONET) is a ground-based federated network of Sun photometer that measures the extinction aerosol optical depth at seven wavelengths (340, 380, 440, 500, 670, 870, and 1020 nm) from the direct Sun measurements over worldwide locations [Holben *et al.*, 1998]. The AOD measurements are accurate to within ± 0.01 at visible wavelengths and ± 0.02 in the near-UV region [Dubovik *et al.*, 2000]. AERONET Sun photometer also measures the spectral diffuse sky radiation at several angles which are inverted in conjunction with the direct Sun measurements to derive the spectral SSA (440, 675, 870, and 1020 nm) and size distribution [Dubovik and King, 2000]. The estimated uncertainty in retrieved SSA is within ± 0.03 for AOD (440 nm) larger than 0.4. This error is largely attributed to the uncertainty in the instrument calibration [Dubovik *et al.*, 2000, 2002]. Also, the AERONET SSA retrieval is expected to be more reliable for moderate to heavy aerosol loading, and at larger solar zenith angle, both produce a stronger absorption signal [Dubovik and King, 2000; Dubovik *et al.*, 2000]. The AERONET- retrieved SSA has been compared with other source of measurements in several studies. For the Indian Ocean Experiment study, Ramanathan *et al.* [2001] have found a good level of agreement in SSA retrieved from AERONET and in situ measurements within the combined uncertainties of the two retrieval techniques. Haywood *et al.* [2003] showed an agreement between the in situ profile measurements of SSA and AERONET retrievals which was within 0.03 at midvisible wavelength for the biomass burning smoke over Namibia. On the other hand, several studies have found disagreement larger than 0.03 between the in situ measurements and AERONET inversion. This has been further discussed in section 4.

Here we use the AERONET-derived Level 2.0 (cloud-screened and quality assured) retrievals of SSA at 440 nm for comparison with the OMAERUV SSA record. AERONET reports the spectral SSA for observations when AOD (440 nm) exceeds 0.4. Therefore, the OMI-AERONET SSA comparison is possible only for AOD larger than 0.4. Beginning in 1993 till present (August 2013), AERONET has operated Sun photometers over an increasing number of sites around the world. As of August 2013, AERONET Sun photometers have provided direct and inverted measurements at about 700 sites globally (source: <http://aeronet.gsfc.nasa.gov>), out of which many sites have aerosol record for several years. Figure 1 (top) shows the global distribution of AERONET sites where at least one daily measurement of Level 2 SSA is available during OMI operation (2004 to present). The color scale is indicative of total number of days having at least one daily SSA inversion with coincident AOD (440 nm) greater than 0.4. A histogram relating the number of AERONET sites with associated number of days shown in the inset reveals that a total of 454 sites satisfy above requirement. For the regional comparison of OMAERUV-AERONET, different regions of the world are considered which are marked with dotted boxes.

2.3. Colocation of OMI and AERONET

2.3.1. Spatial and Temporal Colocation

OMI retrievals correspond to a spatial scale of $13 \times 24 \text{ km}^2$ at nadir and therefore represent the atmospheric conditions over a small region. Unlike the direct measurements of the spectral AOD which are columnar point measurements, the almucantar retrievals made by AERONET use the sky radiances measured at several discrete angles azimuthally. Therefore, the AERONET inversions correspond to sky condition observed over a

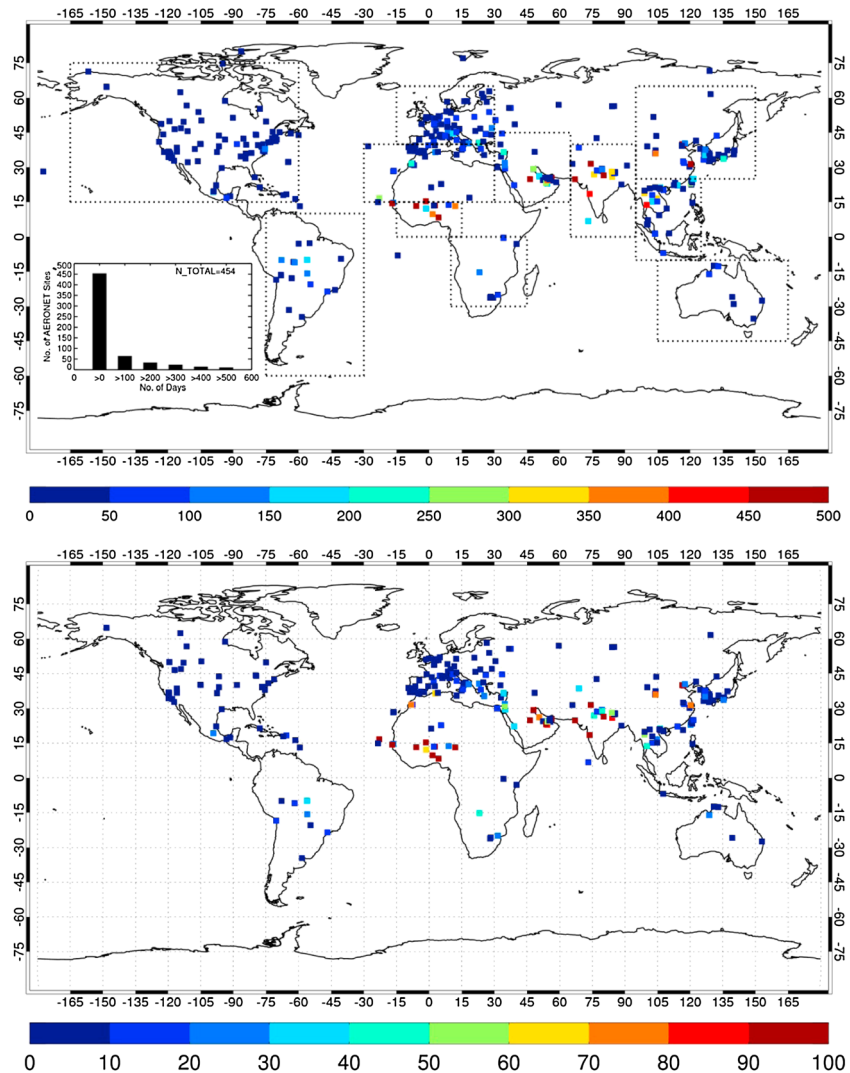


Figure 1. (top) Global distribution of AERONET sites where at least 1 day of Level 2 inversion data is available. The square dots are the geolocation of the sites, and colors represent the availability of inversion data in number of days during the operation period of OMI (October 2004 to August 2013). A histogram relating the number of sites to the respective number of days is shown in the inset. Different regions that are considered in the present OMAERUV versus AERONET analysis are depicted with dotted boxes. (bottom) Global distribution of sites where at least one colocated OMI-AERONET inversion matchup was obtained (refer to section 2.3.1 for the collocation procedure). The color scale represents the number of matchup points for each site.

station which is actually associated with approximately 5 km radius region surrounding the Sun photometer site (T. Eck, NASA GSFC, personal communication, 2013).

In comparison to the direct Sun measurements of AOD which are more frequent and require less stringent atmospheric conditions, the AERONET algorithm performs the almucantar inversion less frequently and requires favorable atmospheric conditions (AOD 440 nm > 0.4 and solar zenith angle > 45°). Moreover, the timings of OMI overpass may not closely overlap with that of AERONET measurements. Additionally, the AERONET almucantar inversions are expected to have better accuracy at large solar zenith angles owing to longer atmospheric path and resultant better absorption signal [Dubovik et al., 2000, 2002]. These conditions are best satisfied for the measurements made during early morning and late afternoon hours, whereas Aura/OMI overpasses a particular station during afternoon hours with the local equator-crossing time 1:30 P.M. Therefore, in order to collocate both types of measurements, one needs to determine a time window around satellite overpass time during which reliable AERONET measurements can be obtained for

temporal averaging. We select a time window of ± 3 h around OMI overpass time in order to get sufficient high-quality AERONET retrievals particularly from early morning/late afternoon measurements. As mentioned above, due to less frequent AERONET almucantar retrieval, the minimum number of measurements required for the collocation was set to unity. Correspondingly, the OMI retrievals of SSA were spatially averaged in a grid area of 0.5° by 0.5° centered at the AERONET site. Though the spatial averaging area for the OMI retrieval is about 50 km^2 , due to its bigger footprint, the actual area intercepted by OMI pixels around AERONET site is likely to be larger. Figure 1 (bottom) shows the distribution of AERONET sites where at least one matchup was obtained following the collocation procedure described above.

OMAERUV algorithm employs three major aerosol types in the retrieval, i.e., carbonaceous or smoke, dust, and urban/industrial. The selection of a particular aerosol type depends on the combination of observed UV-AI and AIRS CO concentration. While averaging valid OMI retrievals in a 0.5° square box, all aerosol types are considered. When all the retrievals were identified as a single aerosol type, then we assign that aerosol type to that particular matchup in the comparison. If more than one aerosol type is identified, then the matchup is referred to as "mixture." Note that originally, the OMAERUV algorithm assumes only a single aerosol type for a particular retrieval and does not consider any mixture.

2.3.2. Wavelength Transformation

AERONET and OMI retrieve aerosol absorption properties in the different regions of the solar spectrum. While AERONET inversion products of the refractive index and single-scattering albedo are available at the visible and shortwave-IR (440, 670, 860, and 1020 nm) wavelengths, OMI performs retrieval at the near-UV wavelengths 354 nm and 388 nm. Though the wavelength difference between the 388 nm (OMI) and 440 nm (AERONET) retrievals is not large (~ 50 nm), knowing that the smoke as well as dust absorptions are wavelength dependent [Russell *et al.*, 2010], both retrievals need to be tied to a reference wavelength for the direct comparison. Currently, the OMAERUV carbonaceous models assume a strong spectral dependence in absorption in the near UV (Absorption Angstrom Exponent (AAE) ~ 2.5 – 3.0) and a neutral dependence between near-UV wavelength (388 nm) and midvisible (500 nm) (AAE ~ 1.0). Results of Kirchstetter *et al.* [2004] and Russell *et al.* [2010] based on the field campaign data show that the aerosol absorption is a continuous function of wavelength and can be approximated as power law with a single value of AAE. In this reference, the sharp discontinuity in the absorption properties of OMI models seems to be less realistic. For the smoke aerosol type, therefore, we assume that the AAE adopted in the smoke models for the near-UV retrieval is also valid for the 388–440 nm narrow spectral range. This allows the wavelength transformation of SSA from near-UV to be visible in two steps: First, the retrieved AOD and AAOD at 388 nm were interpolated to 440 nm following the assumed Extinction AE and Absorption AE, respectively. Second, the SSA at 440 nm now can be computed as

$$\text{SSA} = \frac{\text{AOD} - \text{AAOD}}{\text{AOD}}$$

The OMAERUV dust and urban/industrial models, on the other hand, are characterized with a continuous absorption spectrum from near UV to visible characterized with prescribed values of AAE. Therefore, the 388 nm OMI SSA for these retrievals was directly interpolated to 440 nm by using the values at 388 (retrieved) and 500 nm (converted retrievals). The interpolated OMI SSA values at 440 nm were then directly compared with AERONET SSA at that wavelength.

3. OMI-AERONET Comparison Results

3.1. Biomass Burning Domain

3.1.1. Original Versus Interpolated SSA

Although OMI and AERONET retrieve SSA at different wavelengths, it is worthwhile to initially compare the two sets of retrievals at their native wavelengths for the consistency check. The gap between the shortest wavelength of AERONET (440 nm) and OMI retrievals (388 nm) is only about 50 nm, and therefore, it is expected that the SSA in this spectral region should not vary by a considerable magnitude. The field campaign in situ measurements of spectral SSA reveal the 388–440 nm difference of less than 0.01 for the biomass burning particles (Southern African Fire-Atmosphere Research Initiative (SAFARI) 2000) and up to 0.03 for the dust aerosols (Aerosol Characterization Experiment (ACE)-Asia and Puerto Rico Dust Experiment) [Russell *et al.*, 2010]. Given the uncertainty of ± 0.03 in OMI and AERONET inversions, the remaining differences

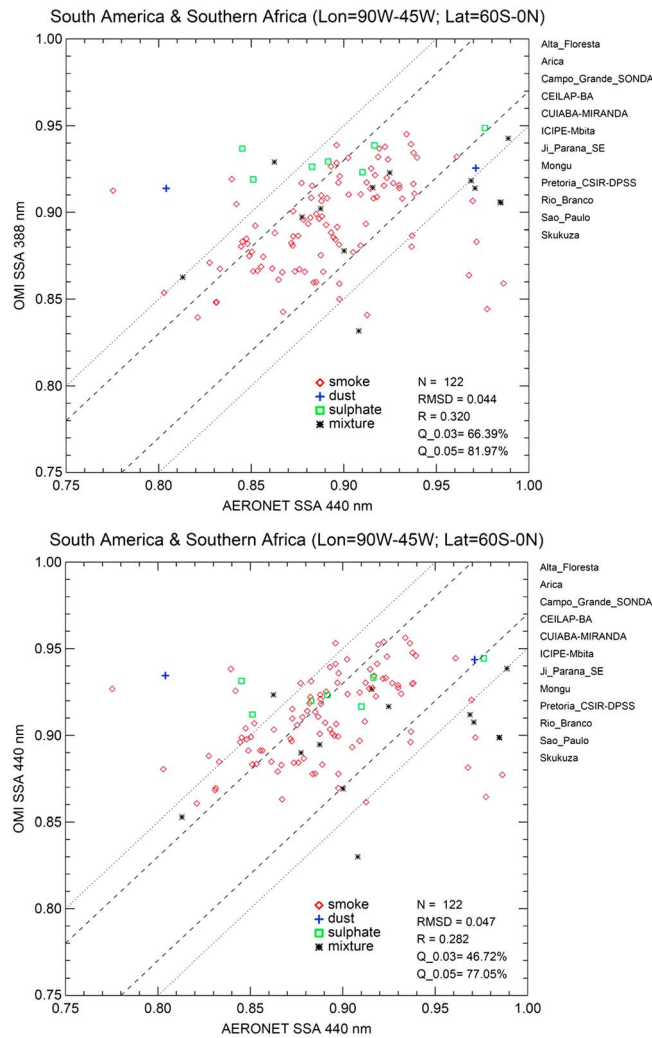


Figure 2. OMAERUV versus AERONET single-scattering albedo comparison at their original retrieved wavelengths, i.e., (top) 388 versus 440 nm and (bottom) at 440 nm wavelength for sites in South America and southern Africa (listed on right side of the plot). OMI values were interpolated from 388 to 440 nm following the model-assumed spectral dependence of aerosol absorption and extinction. Legends with different colors represent the aerosol type selected by the OMAERUV algorithm for the collocated matchups (*N*). RMSD is the root-mean-square difference between the two retrievals; *Q*_{0.03} and *Q*_{0.05} are the percent of total matchups (*N*) that fall within the absolute difference of 0.03 and 0.05, respectively.

Figure 2 (bottom) shows comparison plot for the same sites but for the reference wavelength of 440 nm. Overall, the OMI SSA retrievals at 388 as well as 440 nm (converted) agree within the given uncertainty range of AERONET retrievals (± 0.03). The OMAERUV algorithm selects “smoke” model for most retrievals over these sites. Since these models exhibit strong wavelength dependence in absorption in the near-UV to shortwave visible region of spectrum which act as a proxy for the organics-rich carbonaceous aerosols [Kirchstetter *et al.*, 2004; Jethva and Torres, 2011] and the same dependence (AAE in the range 2.5–.30) was used for the SSA conversion, the 440 nm SSA is found to be higher by 0.01–0.02 than that at 388 nm. The percent of matchups within the predicted uncertainties were higher (root-mean-square difference, RMSD lower) in the original wavelength comparison than that at 440 nm. Since this conversion relies on the current model assumption of the spectral dependence of aerosol extinction and absorption in the near-UV region, the agreement between OMI and AERONET can be affected or improved depending upon the accuracy of

between these two wavelengths may even facilitate this comparison. Also, comparison at original retrieval wavelengths avoids the uncertainty that may be caused by the interpolation from near UV to visible.

Figure 2 (top) shows SSA comparison between OMI (y axis) and AERONET (x axis) at their original wavelengths for the sites located in the biomass burning areas of Amazonia and southern Africa. Both regions undergo intense biomass burning activities during dry season (July–August–September) which eventually emits a large amount of carbonaceous particulate matter in to the atmosphere. In Africa, the major burning activities start in July over northern Savanna and progressively shift to south through September. Using ground-based AERONET inversion, Eck *et al.* [2013] show that the absorption properties of these smoke aerosols exhibit a seasonal trend where the monthly mean aerosol SSA (440 nm) increases significantly from 0.84 in July to 0.93 in November. While there was no significant trend observed in the particle size distribution (fine and coarse mode), the change in SSA was mainly driven by the downward trend in imaginary index. An analysis of the OMI-retrieved SSA (388 nm) in the same paper also showed a similar trend as observed by AERONET and suggest that the seasonal change in SSA is widespread over much of southern Africa. In contrast, there was a very weak or no trend in SSA noted for the sites in southern Amazonia.

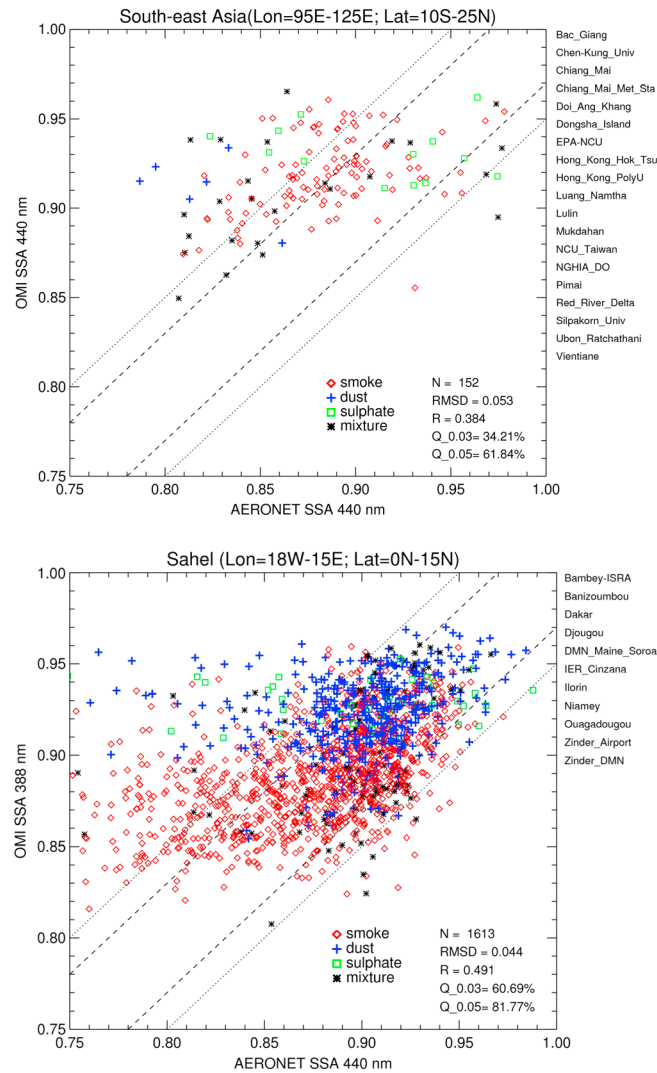


Figure 3. OMAERUV versus AERONET single-scattering albedo comparison at 440 nm for the (top) Southeast Asia and (bottom) Sahel. Legends with different colors represent the aerosol type selected by the OMAERUV algorithm for the co-located matchups (*N*). RMSD is the root-mean-square difference between the two retrievals; *Q*_{0.03} and *Q*_{0.05} are the percent of total matchups (*N*) that fall within the absolute difference of 0.03 and 0.05, respectively. AERONET sites listed on the right side of the plot were used in the present comparison.

3.1.3. Sahel

Sahel and western African regions are major sources of biomass burning smoke during boreal winter. Over this region, the smoke particles generated from burning activities are often mixed with the dust aerosols transported from Saharan desert during dry season. Also, the presence of both dust and smoke either as a single layer or multiple/mixed layers is expected over this region depending upon the time of year and transport pattern [Yang et al., 2013]. At present, however, the OMAERUV algorithm treats this kind of situation as a single layer with a fixed aerosol type identified on the basis of the carbon monoxide and UV aerosol index measured by AIRS and OMI, respectively. Since both dust and smoke aerosols absorb solar radiation in the near-UV region and given the narrow wavelength span between the retrieval channels 354 nm and 388 nm, the impact of the aerosol mixing on the retrieval can be less severe. Nonetheless, such complicated situation should be analyzed through sensitivity analysis in the future. Several AERONET sites over Sahel have

this assumption. The statistical results derived from the OMI versus AERONET comparison at the same wavelength would be more meaningful than at their original wavelengths. Given the short wavelength span between OMI (388 nm) and the shortest wavelength of AERONET (440 nm), we believe that the extrapolation of OMI SSA to 440 nm should not be a major cause of agreement or disagreement. Therefore, we adopt the 440 nm as a reference wavelength for the relative evaluation of OMI SSA retrieval against that of AERONET.

3.1.2. Southeast Asia

Biomass burning over the peninsular Southeast Asia particularly over Thailand, Vietnam, and Laos during spring (February–March) is a major source of carbonaceous aerosols in the world [Streets et al., 2004]. Burning of forest, grassland, and agricultural residue are the known primary burning activities which inject considerable amount of carbonaceous particulate matter into the atmosphere. Figure 3 (top) shows the OMI-AERONET comparison for the Southeast Asia region. The OMAERUV algorithm predominantly selects smoke model for the retrieval during burning period (as expected) for which nearly half of the matchup points fall outside the ± 0.03 AERONET uncertainty. Retrievals with the “urban/industrial” model agreed well for SSA larger than 0.9, however, degrades significantly for lower SSA (more absorption) where OMI retrieves much higher values. Overall, about 34% and 62% matchups are found to be within the absolute difference of ± 0.03 and ± 0.05 , respectively.

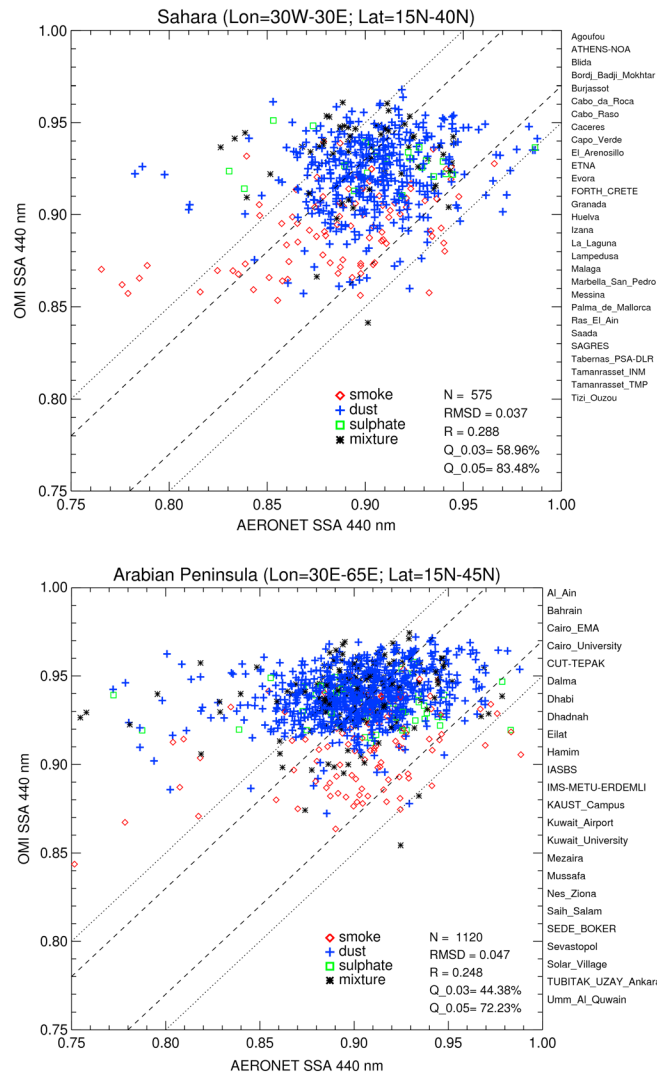


Figure 4. Same as in Figure 3 but for (top) Sahara region and (bottom) Middle East region.

northern Africa including desert sites (*Tamanrasset*, *Zinder_Airport*, *Saada*, and *Blida*), neighboring regions (*Capo_Verde*, *Agoufou*, and *Cairo_EMA*), and Mediterranean sites (*El_Arenosillo*, *Lampedusa*, *Messina*, and *FORTH_CRETE*) have reasonably long record of ground measurements. Sites located in the midst and along the pathways of dust outbreaks are expected to be influenced by the coarse-mode UV absorbing mineral aerosols. Dust plumes from the northern Africa also propagate northward and influence the atmospheric load over Mediterranean region [*Moulin et al., 1998; Prospero et al., 2002*].

Figure 4 (top) shows the comparison of SSA between OMI and AERONET for the Sahara region. As evident from the scatterplot, dust is found to be a dominant aerosol type in the matchups with most points confined to the upper uncertainty limit of ± 0.05 . OMI algorithm also detects smoke over several sites for which the agreement with AERONET is robust with most colocated retrievals falling within the expected uncertainty. For a few matchup points when AERONET retrieves highly absorbing aerosols ($SSA < 0.8$), the OMI smoke (data from *Agoufou*) and dust (*Ras_El_Ain*) retrievals show a relative positive bias.

3.2.2. Arabia Region

Several AERONET sites over the Arabia region including *Bahrain*, *Dhadnah*, *Hamim*, *Kuwait_University*, *KAUST_Campus*, *SEDE_BOKER*, and *Solar_Village* offer multiyear record of aerosol inversion products. Due to

multiyear record of SSA inversion with total number of days exceeding 350. As a result, the total number of matchups between OMI and AERONET are also found to be significantly high ($N > 1500$). Figure 3 (bottom) shows that for smoke aerosols, both retrievals agree with each other well within their expected uncertainties (0.03 and 0.05) for the more frequent range of aerosol absorption ($SSA > 0.82$). For highly absorbing aerosols as retrieved by AERONET ($SSA < 0.82$), OMI tends to retrieve significantly higher SSA. For “dust” and urban/industrial aerosol types, the agreement is reasonable for $AERONET\ SSA > 0.87$, however, degrades considerably for more absorbing aerosols. Overall, about 60% and 81% matchups are restricted within the uncertainty limits of 0.03 and 0.05, respectively.

3.2. Dust Domain

3.2.1. Sahara

During Northern Hemisphere spring and summer, the atmospheric load over Sahara and Arabia region is primarily made up of mineral dust originated from dust outbreaks. The outflow of dust plumes over the Atlantic Ocean is a known phenomenon which has been observed and studied by several satellite-based [*Torres et al., 2002; Kaufman et al., 2005*] as well as ground-based studies. A number of AERONET sites located across the

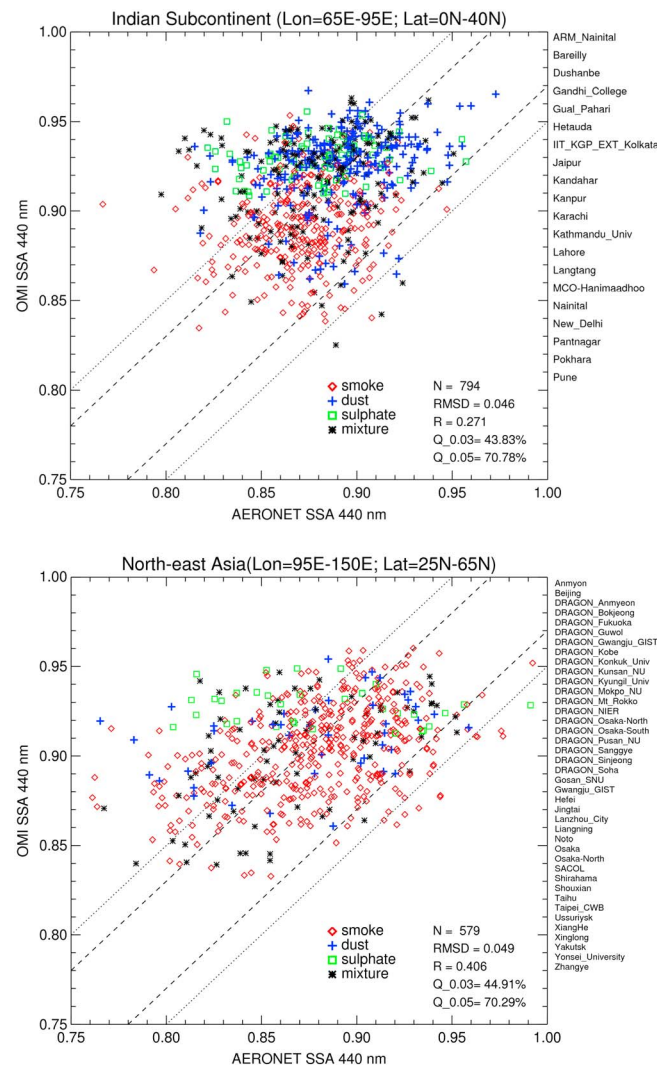


Figure 5. Same as in Figure 3 but for (top) Indian subcontinent and (bottom) North-east Asia region.

vehicular and industrial pollution. During the premonsoon season, however, the region is influenced by the dust transport from the Arabian Peninsula and Thar Desert. In addition to the seasonality of aerosol types and meteorology, vehicular and industrial pollution due to growing population and economic activities increase the atmospheric burden which altogether offers a unique and challenging environment for the satellite algorithms. A number of AERONET sites located over the Indian subcontinent including a decadelong observation over Kanpur provide ground-based measurements for the validation of satellite retrievals. The OMI-AERONET SSA comparison for this region is shown in Figure 5 (top).

For the smoke aerosol types, most OMI retrievals are found to agree with those of AERONET within the uncertainty limits. For dust and urban/industrial retrievals, OMI retrieves SSA mostly in the range 0.9 to 0.95, whereas AERONET exhibits larger range from 0.8 to 0.95. This results in OMI retrieving higher values of SSA compared to AERONET when SSA was lesser than 0.9 as retrieved by AERONET. Despite this bias, overall 70% of the matchups is found to be falling within the ± 0.05 difference.

3.3.2. Northeast Asia

The regions of northeastern China, Korea, and Japan are known to be influenced by the mixture of aerosols. During winter and spring, outbreaks of mineral dust from the Taklimakan and Gobi deserts in northern China and Mongolia region are mobilized under the influence of westerly winds and mix with the local anthropogenic

their proximity to the desert region, the atmospheric load over these sites is expected to be primarily made up of minder dust. However, due to the regional development and the presence of oil industries, emission of carbonaceous particles has also gone up. Figure 4 (bottom) shows that the dust aerosol type dominates in the total matchups for which OMI retrieves significantly higher SSA for AERONET SSA smaller than 0.9. This is also true for matchups in which OMI identifies more than one aerosol type (black asterisk). Sites where OMI-AERONET agreement is found poor are Cairo_EMA, Dhadnah, Kuwait_University, SEDE_BOKER, and Solar_Village. On the other hand, OMI retrievals identified as smoke are found to agree with AERONET within the uncertainties of both inversions. Overall, more than a thousand colocated data points result in RMSD of 0.047 with 44% and 72% of data falling within the differences of ± 0.03 and ± 0.05 , respectively.

3.3. Mixed Environment
3.3.1. Indian Subcontinent

The wintertime blanketing of haze over the northern Indian region has been observed from satellite AOD retrievals and OMI UV absorbing aerosol index. The smoke particles are emitted from agriculture activities including waste burning, biofuel combustion, as well as

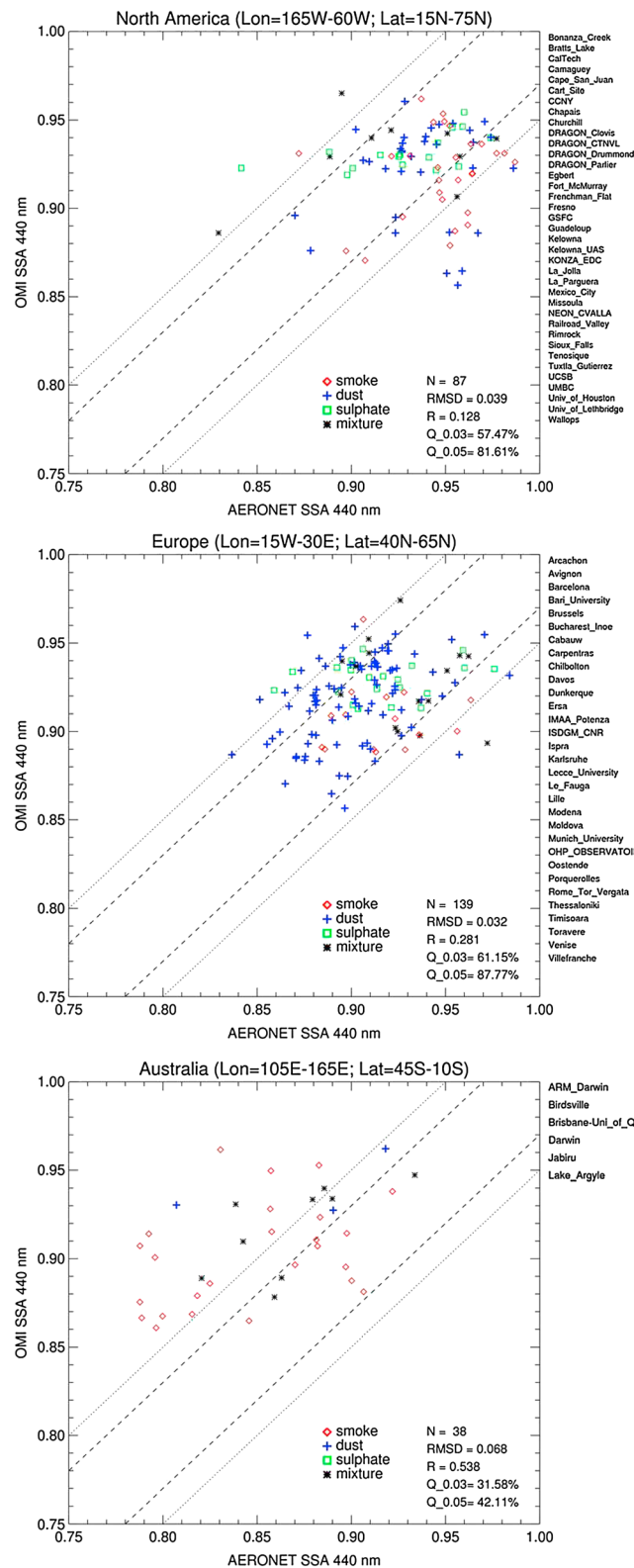


Figure 6. Same as in Figure 3 but for the (top) North America, (middle) Europe, and (bottom) Australia regions.

aerosols generated from the industrial activities, vehicle emissions, and coal burning [Eck et al., 2005]. A number of AERONET sites over this region, therefore, offer a complex environment to evaluate the satellite retrievals. The Gosan SNU site is located over the southern tip of the Jeju Island south of the Korean Peninsula and is expected to be a clean site since there is no major local source of particulate matter in the vicinity of Gosan. However, this site is impacted by the heavy aerosol outflows from the Asian continent, both natural dust as well as anthropogenic pollution, and it was, therefore, considered as one of the super sites for the ACE-Asia 2001 campaign [Kim et al., 2005]. Figure 5 (bottom) shows the OMI-AERONET comparison for the Northeast Asia region. In addition to the permanent AERONET sites, observations from the AERONET's Distributed Regional Aerosol Gridded Observation Network over this region also populate the comparison plot. For smoke-type aerosol retrievals, nearly half of the matchups are found to be within 0.03 with remaining half falling outside the uncertainty envelope. The urban/industrial model retrievals are in good agreement for AERONET SSA > 0.9 but significantly higher for more absorbing aerosols as seen by AERONET. Overall, about 45% and 70% matchups agree within 0.03 and 0.05 uncertainties with RMSD of ~0.05.

3.4. Urban/Industrial Environment: North America, Europe, and Australia

AERONET over North America and Europe comprised a dense network of operating Sun photometers. For the North America region, sites in USA, Canada, Central America, and Caribbean islands are included in the comparison. Sites in USA and Canada spread across the urban centers as well as in remote places and are expected to observe more scattering type of aerosols, whereas Caribbean islands encounter long-range trans-Atlantic dust transport from Sahara during spring and summer [Kaufman et al.,

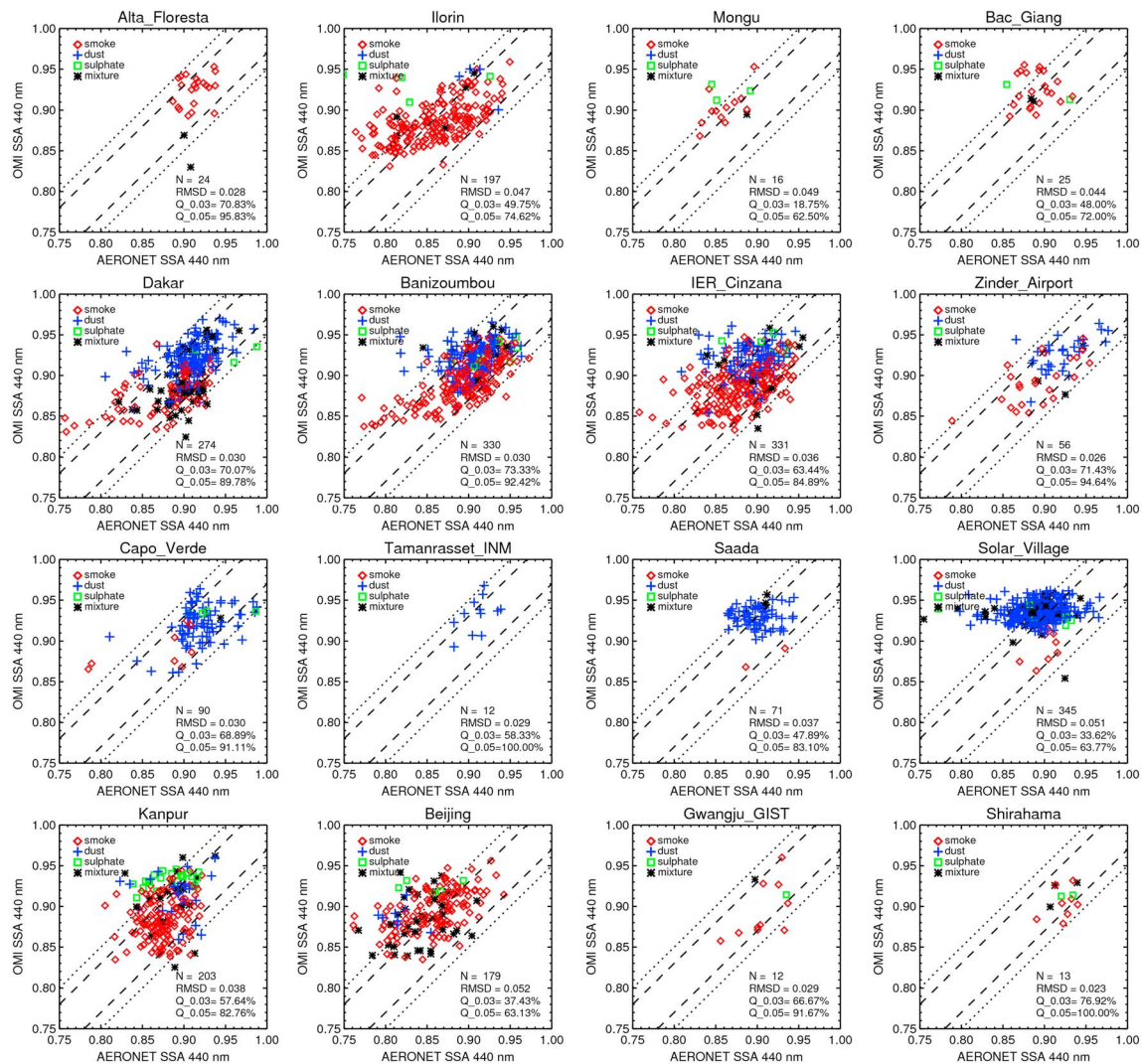


Figure 7. Scatterplots of OMAERUV versus AERONET single-scattering albedo (440 nm) for the representative sites. (top row) Biomass burning-dominated sites, (second row) biomass burning- and dust-dominated sites, (third row) dust sites, and (fourth row) urban locations with seasonal influence of smoke and dust aerosols.

2005]. Sites in Europe are expected to be influenced by urban pollution as well as northward dust transport from the Saharan desert. The Australia continent has a few ground sites located in the Northern Territory, South Australia desert, and on southeast coast. Figure 6 shows the OMAERUV versus AERONET plots for these three regions. For the North America, 57% (82%) of the OMAERUV SSA retrievals agreed to AERONET within the expected uncertainty. While best comparison is found for the urban/industrial and dust aerosols over North America and Europe, the OMAERUV algorithm retrieves significantly higher values of SSA over Australia for the smoke-type retrievals.

The OMAERUV-AERONET comparison for the individual representative sites are shown in Figure 7. The first row presents the scatter plots for the sites *Alta Floresta*, *Ilorin*, *Mongu*, and *Bac Giang* which are representative of the biomass burning aerosols in the South America, Sahel, southern Africa, and Southeast Asia, respectively. The OMAERUV algorithm selects smoke model over these sites and retrieves SSA which is consistent with those of AERONET. The second row shows the comparison for *Dakar*, *Banizoumbou*, *IER_Cinzana*, and *Zinder Airport* which are located in Sahel and Sahara regions. These sites are influenced by the seasonal loading of smoke particles as well as transported dust from Sahara. For both aerosol types, the OMAERUV retrievals are found to be in good agreement with those of AERONET with about 70% (90%) of the collocated points confined to ± 0.03 (± 0.05) level of agreement. The third row shows comparison for the

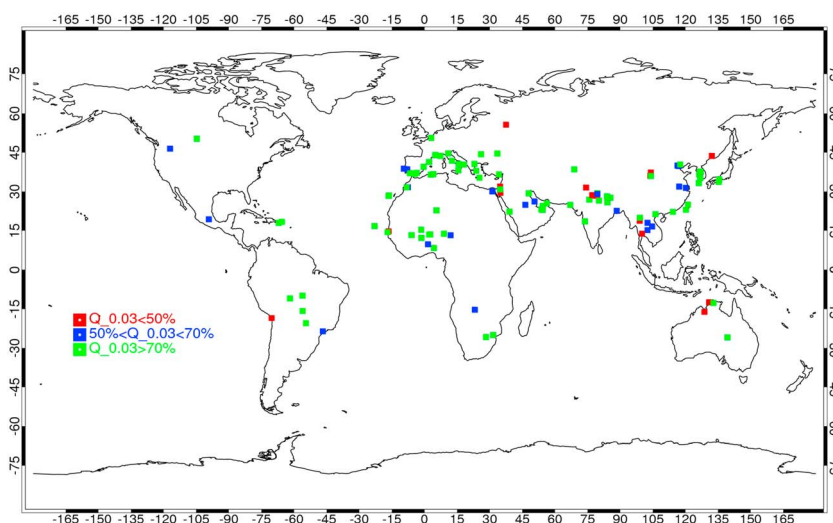


Figure 8. Map of AERONET sites depicted with colors where the color represents % of total OMAERUV versus AERONET matchups that fall within the absolute difference of 0.05.

Capo_Verde, Tamanrasset, Saada, and Solar_Village sites which are primarily influenced by dust aerosols. While most OMAERUV dust retrievals over the former two sites agree well with AERONET, OMI retrieves slightly higher SSA values over site Saada. Over the Solar_Village site in Arabian Peninsula, OMI tends to retrieve much higher than AERONET SSA for dust aerosols. The OMAERUV-AERONET comparison for the Asian sites (fourth row) is found robust over the *Kanpur*, *Gwangju_GIST*, and *Shirahama* sites.

Similar to the site-specific analysis presented above, the statistical results were derived for each individual AERONET site. Figure 8 shows the color coded geographical distribution of the AERONET sites where the color scale represents the % of total matchup for the particular sites that fall within the absolute difference of 0.05. While some isolated stations in the northern part of Australia, Southeast and Northeast Asia, and northern India show moderate to poor agreement between OMI and AERONET, the majority of the sites show consistent retrievals with more than 70% of matchups within the expected uncertainties of the two retrieval techniques.

Table 1 presents the results of the statistical comparison between OMAERUV and AERONET for a number of important sites where total number of matchups was greater than 20. The global composite scatterplot of OMAERUV versus AERONET SSA are shown in Figure 9 (top). All the matchup points obtained from all AERONET sites are combined together to make a composite representation. About 51% and 76% of total matchups are found to be confined within the uncertainties of ± 0.03 and ± 0.05 , respectively. Overall, the agreement between the two sensors is found to be robust for smoke aerosol type then dust and sulphate types.

4. Sources of Uncertainty

4.1. Uncertainty in the Ground-Based AERONET Inversion

The theoretical uncertainty in the AERONET SSA inversion is expected to be within ± 0.03 which arise mainly due to calibration inaccuracy [Dubovik *et al.*, 2000, 2002]. Several field campaign studies have shown by comparing it with the airborne in situ measurements of aerosol absorption that the actual error could be larger than the predicted error of 0.03. Leahy *et al.* [2007] made a direct comparison of the AERONET Level 2 SSA against aircraft-based in situ columnar measurements made for 5 days of SAFARI 2000 campaign and showed that the discrepancies between the two independent observations vary from -0.05 to $+0.03$. It was also noticed that the AERONET Version 2 inversion algorithm retrieves lower SSA compared to those of Version 1 algorithm over bright surfaces. Similar findings were also reported by Haywood *et al.* [2003] for the *Etosha Pan* site where Version 1 of AERONET data provided good agreement (< 0.01) with in situ derived spectral SSA, but Version 2 of AERONET data showed larger discrepancies (> 0.04).

Table 1. OMAERUV Versus AERONET Single-Scattering Albedo (440 nm) Comparison Statistics for Sites With Number of Matchups (N_{MATCHUPS}) Greater Than 20^a

Site	Lon (deg)	Lat (deg)	AOD 440 nm	EAE (440–860 nm)	AAE (440–860 nm)	N_{MATCHUPS}	RMSD	Q_0.03	Q_0.05
Agoufou	−1.48	15.35	0.75	0.19	1.69	180	0.04	61	82
Alta_Floresta	−56.1	−9.87	1.19	1.9	1.42	24	0.03	71	96
Bac_Giang	106.22	21.29	0.82	1.4	1.43	25	0.04	48	72
Bahrain	50.61	26.21	0.58	0.51	1.48	68	0.05	31	59
Bambey-ISRA	−16.48	14.71	0.71	0.29	1.45	28	0.1	7	32
Banizoumbou	2.66	13.54	0.77	0.25	1.75	330	0.03	73	92
Beijing	116.38	39.98	0.81	1.07	1.4	179	0.05	37	63
Blida	2.88	36.51	0.59	0.42	2.1	47	0.05	40	70
Cairo_EMA	31.29	30.08	0.59	0.85	1.42	24	0.06	29	54
Capo_Verde	−22.93	16.73	0.65	0.2	1.9	90	0.03	69	91
Chiang_Mai_Met_Sta	98.97	18.77	1.05	1.64	1.16	43	0.07	12	35
Dakar	−16.96	14.39	0.69	0.28	2.15	274	0.03	70	90
Dhabi	54.38	24.48	0.57	0.57	1.89	24	0.03	58	96
Dhadnah	56.33	25.51	0.6	0.55	1.52	171	0.04	38	73
Djoujou	1.6	9.76	0.89	0.64	1.58	178	0.06	42	60
DMN_Maine_Soroa	12.02	13.22	0.7	0.26	1.46	133	0.06	42	68
Dushanbe	68.86	38.55	0.56	0.52	1.29	28	0.03	61	86
Eilat	34.92	29.5	0.55	0.41	2.26	32	0.06	19	41
Gandhi_College	84.13	25.87	0.78	0.75	1.25	66	0.04	65	82
Gual_Pahari	77.15	28.43	0.76	0.7	1.28	40	0.06	15	40
Hamim	54.3	22.97	0.6	0.35	1.65	72	0.03	61	89
IER_Cinzana	−5.93	13.28	0.73	0.24	1.79	331	0.04	63	85
Ilorin	4.34	8.32	1.15	0.61	1.77	197	0.05	50	75
Jaipur	75.81	26.91	0.55	0.32	2.08	22	0.03	73	91
Kanpur	80.23	26.51	0.76	0.64	1.59	203	0.04	58	83
Karachi	67.03	24.87	0.6	0.52	1.45	177	0.05	40	72
KAUST_Campus	39.1	22.31	0.63	0.36	2	29	0.01	90	100
Kuwait_University	47.97	29.33	0.65	0.36	1.55	92	0.05	49	74
Lahore	74.32	31.54	0.76	0.68	1.56	106	0.06	14	47
Lecce_University	18.11	40.33	0.5	0.55	2.05	26	0.08	50	77
Mezaira	53.78	23.15	0.64	0.38	1.52	85	0.03	79	94
Mussafa	54.47	24.37	0.52	0.44	1.82	51	0.03	57	90
Ouagadougou	−1.4	12.2	0.89	0.31	1.69	58	0.03	69	90
Pantnagar	79.52	29.05	0.65	0.96	1.3	26	0.06	31	50
Pokhara	83.97	28.15	0.6	1.28	1.22	40	0.04	45	73
Pune	73.81	18.54	0.68	1.03	1.24	36	0.05	50	75
Saada	−8.16	31.63	0.53	0.31	1.76	71	0.04	48	83
SACOL	104.14	35.95	0.54	0.69	1.47	40	0.05	55	78
SEDE_BOKER	34.78	30.85	0.62	0.37	1.58	53	0.04	45	79
Solar_Village	46.4	24.91	0.65	0.32	1.77	345	0.05	34	64
Taihu	120.21	31.42	0.83	0.9	1.84	48	0.05	46	60
XiangHe	116.96	39.75	0.82	1.01	1.68	133	0.05	32	65
Xinglong	117.58	40.4	0.72	0.9	1.48	26	0.03	77	88
Zinder_Airport	8.99	13.78	0.7	0.23	1.7	56	0.03	71	95
Zinder_DMN	8.98	13.77	0.7	0.2	1.43	21	0.02	86	100

^aNotations: AOD is the AERONET-measured aerosol optical depth at 440 nm; EAE and AAE are the Extinction and Absorption Angstrom Exponent, respectively, for the wavelength range 440–870 nm; RMSD is the root-mean-square difference of OMI-AERONET SSA; and Q_0.03 and Q_0.05 are the percent of total matchups falling within the absolute difference of 0.03 and 0.05, respectively.

By comparing the AERONET columnar SSA against the equivalent aircraft in situ column-mean estimates over site Banizoumbou under dusty conditions, *Osborne et al.* [2008] found that the Version 2 data of AERONET was lower by 0.03–0.08, whereas Version 1 gave closer agreement with the aircraft-based SSA measurements. However, for the mixture of dust and biomass burning aerosols observed over the Banizoumbou region during Dust and Biomass burning Experiment, *Johnson et al.* [2009] found better agreement (within 0.02) in SSA (500 nm) between the aircraft in situ measurements (SSA = 0.87) and AERONET Version 2 inversion (SSA = 0.85). Note that the Version 1 of AERONET algorithm gave much higher SSA (500 nm) of 0.91 for the Banizoumbou case study. One possible reason for the observed discrepancies between the in situ measurements and AERONET retrievals could be the fact that the in situ measurements represent the SSA of

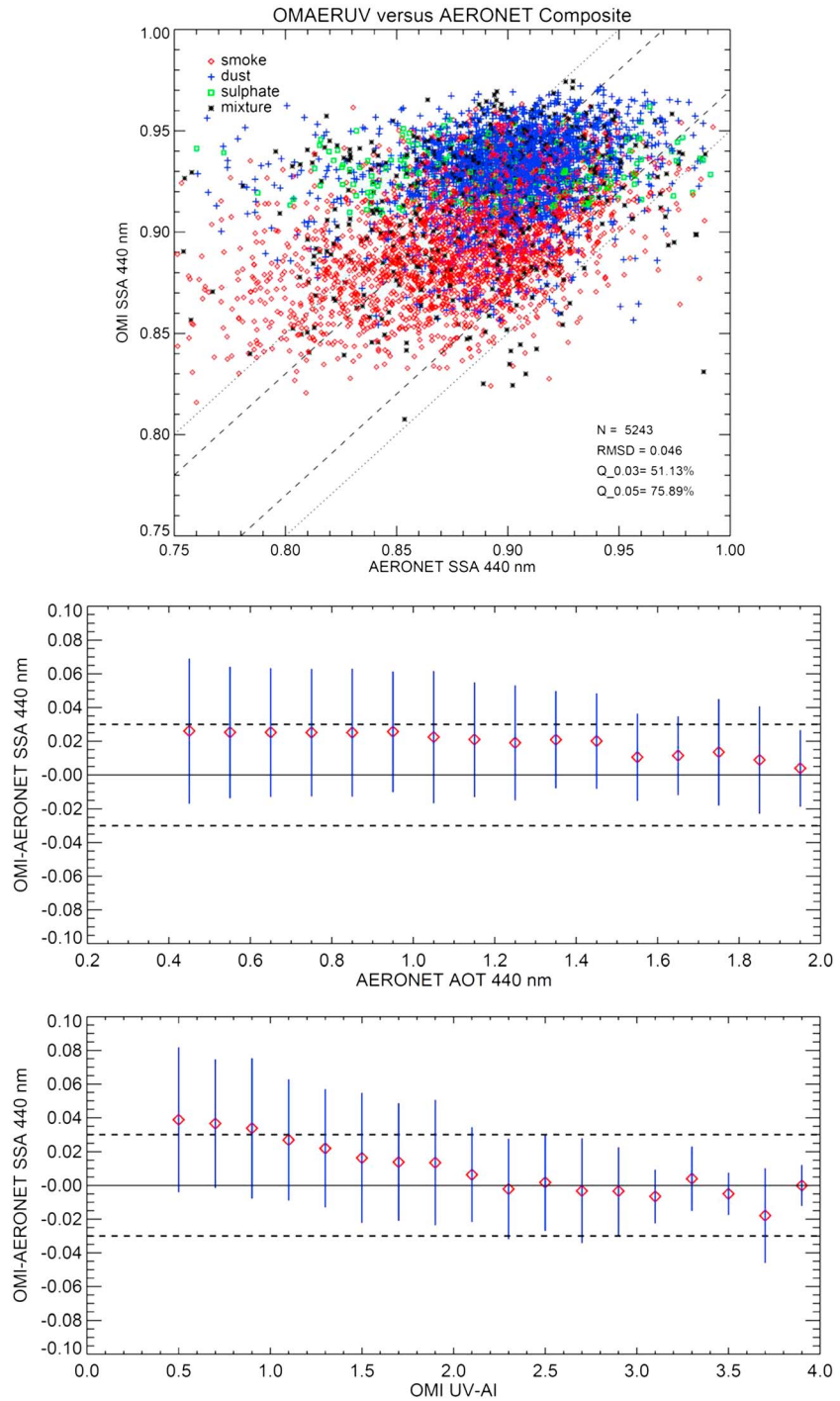


Figure 9. (top) A global composite scatterplot of OMAERUV versus AERONET single-scattering albedo (440 nm). All OMI versus AERONET matchups data obtained from the co-location procedure are used here, and all three aerosol types, i.e., smoke, dust, and urban/industrial, are considered. (middle) Difference in the single-scattering albedo (440 nm) between OMI and AERONET for all the aerosol types as a function of the coincident AERONET-measured aerosol optical depth and (bottom) OMI-measured UV-AI. Red diamonds are the mean of difference for each AOD and UV-AI bin of size 0.1 and 0.2, respectively, whereas vertical lines are the associated standard deviation. The dotted horizontal lines are the expected uncertainties (± 0.03) in the AERONET and OMI SSA inversions.

dehydrated particles, whereas AERONET measures the ambient atmospheric properties of aerosols which can be hygroscopic in nature.

In another comparative study, *Estellés et al.* [2012] treated the AERONET Cimel Sun photometer data collected at *Burjassot* (Valencia, Spain) with the adjusted SKYRAD.pack software developed for the SKYNET ground-based network and retrieved SSA at the AERONET wavelengths of inversion. It was found that although AOD compared well ($\text{RMSD} < 0.01$) between the two software packages for all aerosol burden, the retrieved SSA compared better ($\text{RMSD} \sim 0.03$ at 440 nm) at higher aerosol loading ($\text{AOD} > 0.2$). The difference between the two results was purely attributable to the differences in the inversion codes since identical measurements and calibration were used.

Given the known uncertainty in the AERONET-inverted SSA quantified through several comparative studies discussed above, OMI-AERONET agreement within absolute difference of ± 0.03 under favorable conditions ($\text{AOD} > 0.4$ and solar zenith angle $> 45^\circ$) can be regarded close considering the essentially different ground-based and spaceborne inversion approach. However, OMI-AERONET discrepancies up to 0.05 should not necessarily warrant that satellite-retrieved value is incorrect as large differences between other in situ and AERONET data have been documented by above studies. Factors such as instrumental offset and calibration, uncertain algorithmic assumptions, and atmospheric conditions can affect the accuracy of both ground and satellite retrievals.

4.2. Possible Sources of Uncertainty in OMAERUV Retrieval

Like other satellite-based remote sensing algorithms, OMAERUV also involves standard assumptions about the atmospheric and surface properties. So far, the largest single-known source of error in the OMI retrievals is the subpixel cloud contamination within the OMI footprint. Given the size of footprint of $13 \times 24 \text{ km}^2$, the presence of subpixel clouds may not be completely avoided. Currently, the algorithm assigns quality flags to each pixel which carries information on the quality of the retrieval [*Torres et al.*, 2013]. Aerosol retrieval with quality flag 0 are considered to be the best in accuracy as this category of flag scheme largely avoids cloud contaminated pixels by choosing the appropriate reflectivity and UV-AI thresholds. Over the desert regions, e.g., AERONET sites in the Sahara and the Arabian Peninsula, where large differences in ground-satellite SSA are reported, the frequency of occurrence of clouds is expected to be minimal. Therefore, it is less likely that the SSA retrievals over these sites are affected by cloud contamination. In fact, over ocean where chances of cloud contamination, in general, are higher than over land, e.g., *Capo Verde* site, the OMAERUV dust retrievals are in better agreement with AERONET. The quality flag scheme, however, cannot absolutely rule out the presence of small levels of subpixel cloud contamination or the presence of thin cirrus in the OMI footprint which can cause overestimation in the retrieval of SSA.

Another possible source of uncertainty can be the assumption of the aerosol layer height. The climatology of aerosol layer height derived from CALIOP measurements adequately describes the observed mean layer of carbonaceous and desert dust aerosols [*Torres et al.*, 2013]. It is particularly robust over the arid and semiarid areas where large number of observations was used in calculation. However, note that the temporal and spatial coverage of CALIOP is limited with 16 day repeat cycle over the same location. Variations in the aerosol layer height not observed by CALIOP, therefore, will be missed out in the derived climatology and thus can be a source of uncertainty.

The third source of uncertainty that can affect the SSA retrieval over desert areas is the accuracy of the prescribed surface albedo. The surface in the OMAERUV algorithm is assumed to be Lambertian and is characterized by a $1^\circ \times 1^\circ$ monthly climatology originally derived from the Total Ozone Mapping Spectrometer (TOMS) long-term measurements. The climatology of near-UV surface albedo is essentially derived following the minimum reflectivity approach and is expected to be accurate within 0.005 to 0.01. The sensitivity of the OMAERUV retrieval to the surface albedo perturbation is discussed in section 4.4.

The assumed aerosol microphysical and optical properties could be additional sources of uncertainty. The particle size distributions assumed in the OMAERUV models are adopted from long-term AERONET inversion statistics [*Dubovik et al.*, 2002] and are considered realistic representations of the total atmospheric column. A one-to-one comparison of the relative spectral dependence in absorption in the UV to visible region between the OMAERUV dust model and in situ measurements for site *Cairo* reported in the work of *Wagner et al.* [2012] reveals that the AAE produced by these two data sets are consistent. Both data sets exhibit a

large value of AAE in the wavelength range 300–700 nm for dust aerosols with *Wagner et al.* [2012] and OMAERUV AAE being 2.50 and 2.94, respectively. The spectral dependence measured over the other sites of the Saharan Mineral Dust Experiment, however, were weaker than that assumed in the OMAERUV algorithm. Although the currently assumed spherical shape of dust particles and remaining uncertainty in the relative spectral dependence of the imaginary component of the refractive index still could be potential sources of uncertainty, the better AERONET-OMI SSA agreement over the oceans than over land is not consistent with a systematic dust aerosol model-related error.

Several studies have shown that the mineral dust aerosols are, in general, nonspherical in shape which exhibit different phase functions than the pure spherical particles at scattering angle viewed by the satellites [*Mishchenko et al.*, 1995, 1997]. Satellite retrievals such as from Moderate Resolution Imaging Spectroradiometer (MODIS) [*Levy et al.*, 2007] and Multiangle Imaging Spectroradiometer [*Kalashnikova et al.*, 2011] have shown a marked improvement in the retrieval of dust AOD by incorporating the effects of nonspherical dust aerosols into the algorithm. For the UV region of the spectrum, such studies are very limited. *Krotkov et al.* [1999] found significant difference in the simulated 340–380 nm spectral contrast between randomly oriented spheroids and spherical particles for volcanic ash particles in the scattering angle range 90°–150°. Due to larger backscattering at these viewing geometries, spherical treatment of these nonspherical particles may result in overestimated AOD as well as SSA. On the other hand, a significant amount of Rayleigh scattering in the near-UV region particularly for the atmosphere above the aerosol layer may also smears out the effect of aerosol phase function on the top-of-atmosphere signal. For the present colocated global matchups between OMI and AERONET, the difference in SSA for carbonaceous and dust aerosols apparently did not show a clear relationship with the scattering angle in the range where nonspherical particles can have effects on the retrieval. This relationship remained largely inconclusive. The effects of the shape of the particles on the radiances and consequently on the retrieval become even more complicated when the spherical and nonspherical particles are mixed in the real atmosphere for which the use of just one model would result in the erroneous retrieval [*Wang et al.*, 2003]. Nevertheless, the effects of shape of the dust particles should be further investigated in the future version of the OMAERUV upgrade.

The carbonaceous aerosol models are characterized with a steep absorption gradient in the near UV to adequately represent the organics in the biomass burning smoke particles. The relative spectral dependence of imaginary index between the retrieval wavelength 354 and 388 nm is assumed to be 20% which translates into the AAE in the range 2.5–3.0 depending on the submodels [*Jethva and Torres*, 2011]. This recent modification in the model properties was supported by the ground-based in situ measurements of spectral absorption carried out over southern Africa region during SAFARI 2000 experiment [*Kirchstetter et al.*, 2004]. Due to the shortage of ground-based characterization of absorption particularly for the near-UV part of the spectrum, the regional representation of the spectral absorption properties in the OMAERUV models is limited. The algorithm currently assumes same spectral dependence for each aerosol type for all the regions in the operational retrieval. Therefore, spatial and temporal variations in the actual aerosol spectral properties can be a potential source of error in the SSA retrieval. A sensitivity analysis of the OMAERUV retrievals to the major source of uncertainties discussed above is presented in section 4.4.

4.3. Diagnosis of OMAERUV Versus AERONET

The AERONET algorithm inverts the spectral sky radiances in conjunction with the direct AOD measurements to retrieve the refractive index (real and imaginary) and particle size distribution under favorable atmospheric conditions. The imaginary index and subsequent SSA inversions are believed to be more stable within the ± 0.03 accuracy for AOD (440 nm) and solar zenith angle greater than 0.4 and 45°, respectively. At larger aerosol loading and for slant path measurements, the inversion is expected to be more robust and accurate owing to stronger absorption signal. Similarly, a sensitivity analysis of the two-channel OMAERUV retrievals suggests that the retrieved AOD and SSA are more susceptible to the small change in surface albedo at lower aerosol loading. For instance, an absolute change of 0.01 in the surface albedo leads to an approximate change in AOD by 0.1 and SSA by about 0.02.

Figure 9 (middle) shows the absolute difference in SSA between OMI and AERONET as a function of concurrent AERONET direct AOD (440 nm) measurements for all aerosol types as identified by the OMAERUV algorithm. All OMI-AERONET matchups data obtained from a total of 269 sites are used here. The diamond symbols and vertical lines represent the mean and 1 standard deviation (1σ) for each AOD bin of size 0.1. Combined all

three aerosol types, the SSA difference plot reveals a clear relationship with the magnitude of AOD where both retrievals gradually converge at increasing aerosol loading. The mean of differences between the two sensors remains less than 0.03 for AOD larger than 0.4, though OMAERUV is slightly biased high at lower aerosol loading. Both sensors, however, converge to even better agreement as aerosol loading increases. When segregated with regard to the aerosol type, smoke and dust aerosol retrievals combined (not shown separately) yield positive mean differences for all AOD bins with all mean values falling well within the known uncertainty of AERONET, i.e., ± 0.03 . For the urban/industrial aerosol type, OMI tends to retrieve much higher value of SSA with a mean and standard deviation of difference to be larger than +0.03.

Figure 9 (bottom) shows a similar plot of SSA difference against the concurrent OMI UV-AI. Notably, the differences in SSA exhibit even a stronger relationship to UV-AI than that in the AOD case (top). For UV-AI lesser than unity, the differences in the retrieval are found to be beyond the expected uncertainty in both inversions. For the lower range of UV-AI, OMI algorithm mostly employs the urban/industrial model for the retrieval where all aerosols are assumed to be confined within the boundary layer (< 2 km) with a vertical profile that follows an exponential distribution. The concurrent AOD measurements from AERONET also showed lower aerosol loading ($AOD < 0.7$) at lower UV-AIs. On the other hand, for UV-AI larger than unity, all the binned values of the SSA difference fall within the 0.03 uncertainty range. The differences approach to zero with reduced spread of matchups as UV-AI attains larger magnitudes. Particularly, both inversions are found to be in near-to-perfect agreement for UV-AI greater than 2.0.

4.4. Sensitivity Analysis of OMAERUV Retrieval

For the sensitivity study, we employ the standalone research version of the OMAERUV code which is equivalent to its operational counterpart. The code requires observed radiances, aerosol layer height information, surface albedo, and geometry parameters to retrieve a pair of AOD and SSA at 388 nm which then converted to 354 and 500 nm assuming the model-dependent spectral extinction and absorption. A few selected outliers from the global OMAERUV versus AERONET matchup plot that represent sites located in different environments, i.e., smoke, dust, and urban were chosen for this analysis. Table 2 lists the site names along with the time of coincidence and retrieved parameters from AERONET and OMI. In order to avoid the retrieval issues associated with subpixel cloud contamination, we select only those outliers for which no clouds around the AERONET sites were detected in the MODIS true color red-green-blue subset image over each selected site. These images were obtained from <http://lance-modis.eosdis.nasa.gov/imagery/subsets/?project=aeronet>. For each coincidence, the OMAERUV research code was first ran with the identical input parameters and look-up table that are being used in the operational code. We find that the output retrieval from the research code agree with those of operational code within the absolute difference of 0.05 and 0.01 for AOD and SSA, respectively. The remaining differences can be attributed to the minor differences in the numerical interpolation scheme and nodes in geometry.

The OMAERUV algorithm assumes a set of parameters in the retrieval which include spectral dependence of aerosol extinction and absorption, surface albedo, and aerosol layer height. We analyze the impact of each of these parameters on the retrieved AOD and SSA. Table 2 presents the result of this analysis for a few selected cases of OMI-AERONET comparison. For the two case study retrievals over the site Ilorin, the standard OMAERUV retrieves significantly higher SSA ($\Delta\omega \sim 0.09$) and lower AOD (388 nm) using the existing carbonaceous aerosol model. This model assumes a strong spectral dependence in absorption ($AAE \sim 2.8$) in the near-UV range. Retrieval of AOD and SSA using smoke model with AAE of 1.90 (10% relative spectral dependence in the imaginary index between 354 and 388 nm) and 1.0 (no spectral dependence in the imaginary index) bring down the difference in SSA to 0.04 and 0.02, respectively, along with the improved AOD. For the retrieval case over site Mongu in southern Africa, using the smoke model with an AAE of 1.90 provides SSA (440 nm) which is identical to the coincident AERONET value. For the two retrieval outliers over Southeast Asia (Bac_Giang site) for which OMI retrieves higher (lower) values of SSA (AOD), use of smoke model with AAE of unity results in lower SSA which is in better agreement with AERONET within the expected uncertainty. The associated retrieval of AODs shows significant improvement where the new retrieved values at 388 nm are now higher than the AERONET AOD (440 nm) as it is expected that the AOD at shorter wavelength would be larger for the fine-mode carbonaceous aerosols.

Table 2. Sensitivity Results of the OMI Aerosol Retrieval to the Major Algorithmic Assumptions^a

ANET Site	Year	Month	Date	OMI ω_{440}	ANET ω_{440}	$\Delta\omega$	ANET τ_{440}	OMI τ_{388}	UVAI	Aerosol Type	Algorithmic Changes	SIM τ_{388}	SIM ω_{440}
Ilorin	2006	12	21	0.88	0.79	0.09 0.04 0.02	0.92	0.52	0.99	SMK	Model: SMOKE AAE = 1.90 Model: SMOKE AAE = 1.0 RS354 + 0.01; RS388 - 0.01	0.64 1.26	0.83 0.81
Ilorin	2008	1	9	0.89	0.80	0.09 0.04	1.14	0.89	1.20	SMK	Model: SMOKE AAE = 1.90	1.23	0.84
Mongu	2006	8	24	0.90	0.86	0.04 0.00	1.57	1.32	1.07	SMK	Model: SMOKE AAE = 1.90	1.75	0.86
Bac_Giang	2006	12	29	0.95	0.90	0.05 0.01	2.20	1.25	0.66	SMK	Model: SMOKE AAE = 1.0 (BC)	2.77	0.89
Bac_Giang	2007	2	2	0.95	0.88	0.07 0.02	1.26	1	0.75	SMK	Model: SMOKE AAE = 1.0 (BC)	1.80	0.90
Kanpur	2012	11	30	0.92	0.82	0.1 0.06	1.2	1.02	0.85	SMK	Model: SMOKE AAE = 1.90 RS354 - 0.01 RS388 + 0.01	1.48	0.88
Banizoumbou	2007	5	27	0.92	0.88	0.04 0.03	1.21	0.96	1.96	DST	Model: DUST RS354 + 0.01 Model: DUST Aer.Hgt. = 1.5 km	1.17 1.36	0.91 0.89
IER_Cinzana	2005	1	25	0.85	0.77	0.08 0.03	1.09	0.97	2.06	SMK	Model: SMOKE AAE = 1.90 RS354 + 0.01 RS388 + 0.01	1.12	0.80
Saada	2008	6	24	0.93	0.87	0.06 0.04	0.62	0.71	1.48	DST	Model: DUST RS354 + 0.01	0.87	0.91
Solar Village	2008	6	12	0.93	0.83	0.10 0.09	0.81	1.07	1.58	DST	Model: DUST RS354 + 0.01	1.21	0.92

^aNomenclature: ω_{440} single-scattering albedo at 440 nm; $\Delta\omega$: absolute difference in SSA (OMI-ANET); τ_{440} , τ_{388} : aerosol optical depth at 440 and 388 nm; SIM τ_{388} and SIM ω_{440} are the retrieved AOD and SSA using the research version of the OMAERUV algorithm; SMK: carbonaceous aerosol model; and DST: dust model.

For the dust case over site Banizoumbou, while an increase in the surface albedo at 354 nm by +0.01 improves the SSA comparison marginally, change in aerosol layer height from 3 km to 1.5 km significantly improves agreement in both SSA and AOD retrievals against those of AERONET. Similarly, an increase in surface albedo by 0.01 over Saharan site (Saada) and Arabian Peninsula (Solar_Village) showed a decrease in the magnitude of retrieved SSA ($\Delta \sim 0.02$), however, still found insufficient to explain larger differences between OMI and AERONET. To further analyze the impact of surface albedo on the satellite retrieval, all the matchup points for desert stations Saada and Hamim were reprocessed with the increased surface albedo by 0.01 and 0.02. A comparison of new set of results with AERONET retrievals reveals that although the OMI-AERONET differences in retrieved SSA decrease with an increase in the surface albedo, the modeled surface uncertainty effect does not explain the totality of the large discrepancy between the two sensors. On the basis of above results, we suggest that the aerosol models and surface albedo climatology assumed in the OMAERUV algorithm need to be revalidated using the global long-term AERONET measurements and more recent OMI observations of surface albedo. Particularly, the regional representation of the spectral aerosol absorption in the near UV in both biomass burning and dust regions and surface characteristics over the Sahara and Arabian Desert regions are the two components of the algorithm which demand further attention.

5. Summary and Conclusion

We present the first global comparison analysis of the aerosol SSA retrieved from the OMI's two-channel aerosol algorithm (OMAERUV) in relation to the equivalent inversion made by the AERONET Sun photometers across the globe. This study follows a recent upgrade of the OMAERUV algorithm (Version 1.4.2) in which major modifications have been incorporated including use of the new carbonaceous aerosol models, a CALIOP-based aerosol layer height climatology, and a robust aerosol-type identification by taking help of concurrent AIRS CO observations. Since the SSA inferred from two different platforms are essentially retrieved from two fundamentally different inversion algorithms, the present study does not stand as a "validation" exercise for either retrieval data sets. Instead, the purpose of this analysis was to check the consistency between the two retrieved quantities of the same physical parameter in terms of standard statistical comparison, i.e., RMSD and % of matchups within the expected uncertainties.

We include all the AERONET sites that were in operation during OMI period (2004 till August 2013) in this analysis. The collocation procedure that matched temporal inversion data from AERONET with spatial retrievals from OMI gave us a total of 5463 collocated data points collected from 269 sites across the globe that cover major biomass burning regions, deserts, and urban/industrial domains. Note that AERONET retrieves the spectral SSA when AOD (440 nm) exceeds 0.4. Therefore, we could not compare OMI with AERONET for lower AOD conditions in the present analysis. However, OMI retrievals can be compared against other in situ measurements for lower aerosol loading if such data set is available. Globally, 49% (AOD < 0.7) and 53% (AOD > 0.7) of the total OMAERUV-AERONET single-scattering albedo (440 nm) retrievals are found to be in agreement within their estimated uncertainties of ± 0.03 . The agreement improves to 74% and 79%, respectively, when the uncertainty limit was relaxed up to ± 0.05 . The disagreement between the two data sets was significant (~ 0.05) where AERONET (OMAERUV) retrieves much lower (higher) SSA (<0.85). When segregated by aerosol type and region, the agreement between the two sensors is found to be robust over the regions of South America, Sahel, and northern India during biomass burning season. Over the desert sites of Sahara, both data sets are in a reasonable agreement with about 59% (89%) of the matchups falling within the absolute difference of ± 0.03 (± 0.05). AERONET sites over the Arabian Peninsula showed poor comparison in SSA for the dust-type aerosols where OMAERUV retrieved much higher values of SSA for absorbing aerosols as retrieved by AERONET. The smoke- and urban-/industrial-type retrievals were, however, found to be in better agreement over these sites. The OMAERUV smoke-type retrievals over Southeast and Northeast Asia tend to be higher than those of AERONET; however, reasonable number of matchups falls within the 0.03 uncertainty limit. Over Europe, the OMAERUV-AERONET agreement is found to be robust with 61% and 88% of matchups fall within the difference of 0.03 and 0.05, respectively.

Globally, though OMI and AERONET SSA inversions agree reasonably well within their expected uncertainties, the disagreement between the two data sets remains over certain regions. In particular, inconsistent dust

retrievals over Arabian Peninsula, biomass burning retrievals over Southeast Asia and Australia, and retrievals over urban/industrial sites demand further attention. Much of the observed inconsistency is found to occur at moderate to lower aerosol loading ($\text{AOD } 440 \text{ nm} < 0.7$) for which both inversion techniques might have issues related to signal-to-noise ratio and algorithmic assumptions. For instance, the OMAERUV retrievals are more susceptible to the changes in surface albedo at low AODs and to spectral absorption at high AODs. The aerosol models used in the current version of the OMAERUV algorithm were derived from the AERONET measurements documented in the work of Dubovik *et al.* [2002]. Since then, AERONET has expanded its network by installing hundreds of Sun photometers over the diverse regions of the globe. This invaluable data set provides an unprecedented long record of aerosol measurements that is adequate to construct the dynamic aerosol models for the satellite retrievals. In addition to this, there is a need to revalidate the OMAERUV surface albedo climatology using more recent multiyear near-UV observations from OMI. Note that OMI provides higher pixel resolution ($13 \times 24 \text{ km}^2$) than TOMS ($40 \times 40 \text{ km}^2$) and also concurrent to the MODIS operation period, therefore, offers a better surface characterization through A-train synergy.

Despite the remaining uncertainties in both inversions, a reasonable agreement between the two independent techniques globally and, in fact, a robust agreement over many important sites of biomass burning, dust, and urban environment increase the confidence and credibility of the OMAERUV aerosol product which stands uniquely in characterizing aerosol absorption from space.

Acknowledgments

We thank NASA GES-DISC for the online availability of the OMI aerosol products at http://disc.sci.gsfc.nasa.gov/Aura/data-holdings/OMI/omaeruv_v003.shtml. We also thank all the PIs and their staff for establishing and maintaining a number of AERONET sites whose data were used in this investigation. The AERONET data set can be obtained from <http://aeronet.gsfc.nasa.gov/>. The first author would like to thank NASA's EOSDIS LANCE team for their online visualization tool of MODIS subset over AERONET sites which can be accessed at <http://lance-modis.eosdis.nasa.gov/imagery/subsets/?project=aeronet>. We also thank the three anonymous reviewers for their valuable suggestions which have helped in improving the quality of paper.

References

- Ahn, C., O. Torres, and P. K. Bhartia (2008), Comparison of Ozone Monitoring Instrument UV Aerosol Products with Aqua/Moderate Resolution Imaging Spectroradiometer and Multiangle Imaging Spectroradiometer observations in 2006, *J. Geophys. Res.*, *113*, D16S27, doi:10.1029/2007JD008832.
- Ahn, C., O. Torres, and H. Jethva (2014), Assessment of OMI near-UV aerosol optical depth over land, *J. Geophys. Res. Atmos.*, *119*, doi:10.1002/2013JD020188.
- Dubovik, O., and M. D. King (2000), A flexible inversion algorithm for retrieval of aerosol optical properties from Sun and sky radiance measurements, *J. Geophys. Res.*, *105*(D16), 20,673–20,696, doi:10.1029/2000JD900282.
- Dubovik, O., A. Smirnov, B. N. Holben, M. D. King, Y. J. Kaufman, T. F. Eck, and I. Slutsker (2000), Accuracy assessments of aerosol optical properties retrieved from Aerosol Robotic Network (AERONET) Sun and sky radiance measurements, *J. Geophys. Res.*, *105*(D8), 9791–9806, doi:10.1029/2000JD900040.
- Dubovik, O., B. N. Holben, T. F. Eck, A. Smirnov, Y. J. Kaufman, M. D. King, D. Tanre, and I. Slutsker (2002), Variability of absorption and optical properties of key aerosol types observed in worldwide locations, *J. Atmos. Sci.*, *59*, 590–608.
- Eck, T. F., *et al.* (2005), Columnar aerosol optical properties at AERONET sites in central eastern Asia and aerosol transport to the tropical mid-Pacific, *J. Geophys. Res.*, *110*, D06202, doi:10.1029/2004JD005274.
- Eck, T. F., *et al.* (2013), A seasonal trend of single scattering albedo in southern African biomass-burning particles: Implications for satellite products and estimates of emissions for the world's largest biomass-burning source, *J. Geophys. Res. Atmos.*, *118*, 6414–6432, doi:10.1002/jgrd.50500.
- Estellés, V., M. Campanelli, M. P. Utrillas, F. Expósito, and J. A. Martínez-Lozano (2012), Comparison of AERONET and SKYRAD4.2 inversion products retrieved from a Cimel CE318 sunphotometer, *Atmos. Meas. Tech.*, *5*, 569–579, doi:10.5194/amt-5-569-2012.
- Hansen, J., M. Sato, and R. Ruedy (1997), Radiative forcing and climate response, *J. Geophys. Res.*, *102*(D6), 6831–6864, doi:10.1029/96JD03436.
- Haywood, J., P. Francis, O. Dubovik, M. Glew, and B. Holben (2003), Comparisons of aerosol size distributions, radiative properties and optical depths determined by aircraft observations and sun photometers during SAFARI 2000, *J. Geophys. Res.*, *108*(D13), 8471, doi:10.1029/2002JD002250.
- Holben, B. N., *et al.* (1998), AERONET—A federated instrument network and data archive for aerosol characterization, *Rem. Sens. Env.*, *66*(1), 1–16, doi:10.1016/S0034-4257(98)00031-5.
- Intergovernmental Panel on Climate Change (2007), Climate change 2007: The physical science basis, in *Contribution of Working Group I to the Fourth Assessment Report of the Intergovernmental Panel on Climate Change*, edited by S. Solomon *et al.*, Cambridge Univ. Press, Cambridge, U. K., and New York.
- Jethva, H., and O. Torres (2011), Satellite-based evidence of wavelength-dependent aerosol absorption in biomass burning smoke inferred from Ozone Monitoring Instrument, *Atmos. Chem. Phys.*, *11*, 10,541–10,551, doi:10.5194/acp-11-10541-2011.
- Johnson, B. T., S. Christopher, J. M. Haywood, S. R. Osborne, S. McFarlane, C. Hsu, C. Salustro, and R. Kahn (2009), Measurements of aerosol properties from aircraft, satellite and ground-based remote sensing: A case-study from the Dust and Biomass-burning Experiment (DABEX), *Q. J. R. Meteorol. Soc.*, *135*, 922–934, doi:10.1002/qj.420.
- Kalashnikova, O. V., *et al.* (2011), Capabilities of MISR aerosol retrievals in dust-laden conditions, Proceedings of the SPIE Europe Remote Sensing, 8177, doi:10.1117/12.897773.
- Kaufman, Y. J., I. Koren, L. A. Remer, D. Tanré, P. Ginoux, and S. Fan (2005), Dust transport and deposition observed from the Terra-Moderate Resolution Imaging Spectroradiometer (MODIS) spacecraft over the Atlantic Ocean, *J. Geophys. Res.*, *110*, D10S12, doi:10.1029/2003JD004436.
- Kim, S.-W., S.-C. Yoon, A. Jefferson, J. A. Ogren, E. G. Dutton, J.-G. Won, Y. S. Ghim, B.-I. Lee, and J.-S. Han (2005), Aerosol optical, chemical and physical properties at Gosan, Korea during Asian dust and pollution episodes in 2001, *Atmos. Environ.*, *39*(1), 39–50.
- Kirchstetter, T. W., T. Novakov, and P. V. Hobbs (2004), Evidence that the spectral dependence of light absorption by aerosols is affected by organic carbon, *J. Geophys. Res.*, *109*, D21208, doi:10.1029/2004JD004999.
- Krotkov, N. A., D. E. Flittner, A. J. Krueger, A. Kostinski, C. Riley, W. Rose, and O. Torres (1999), Effect of particle non-sphericity on satellite monitoring of drifting volcanic ash clouds, *J. Quant. Spect. Rad. Transf.*, *63*(2-6), 613–630, doi:10.1016/S0022-4073(99)00041-2.

- Leahy, L. V., T. L. Anderson, T. F. Eck, and R. W. Bergstrom (2007), A synthesis of single scattering albedo of biomass burning aerosol over southern Africa during SAFARI 2000, *Geophys. Res. Lett.*, *34*, L12814, doi:10.1029/2007GL029697.
- Lee, K.-H., Z. Li, M.-S. Wong, J. Xin, W.-M. Hao, and F. Zhao (2007), Aerosol single scattering albedo estimated across China from a combination of ground and satellite measurements, *J. Geophys. Res.*, *112*, D22S15, doi:10.1029/2007JD009077.
- Levy, R. C., L. A. Remer, S. Mattoo, E. F. Vermote, and Y. J. Kaufman (2007), Second-generation operational algorithm: Retrieval of aerosol properties over land from inversion of Moderate Resolution Imaging Spectroradiometer spectral reflectance, *J. Geophys. Res.*, *112*, D13211, doi:10.1029/2006JD007811.
- Mishchenko, M. I., A. A. Lacis, B. E. Carlson, and L. D. Travis (1995), Nonsphericity of dust-like tropospheric aerosols: Implications for aerosol remote sensing and climate modeling, *Geophys. Res. Lett.*, *22*, 1077–1080, doi:10.1029/95GL00798.
- Mishchenko, M. I., L. D. Travis, R. A. Kahn, and R. A. West (1997), Modeling phase functions for dustlike tropospheric aerosols using a shape mixture of randomly oriented polydisperse spheroids, *J. Geophys. Res.*, *102*(D14), 16,831–16,847, doi:10.1029/96JD02110.
- Moulin, C., et al. (1998), Satellite climatology of African dust transport in the Mediterranean atmosphere, *J. Geophys. Res.*, *103*(D11), 13,137–13,144, doi:10.1029/98JD00171.
- Osborne, S. R., B. T. Johnson, J. M. Haywood, A. J. Baran, M. A. J. Harrison, and C. L. McConnell (2008), Physical and optical properties of mineral dust aerosol during the Dust and Biomass-burning Experiment, *J. Geophys. Res.*, *113*, D00C03, doi:10.1029/2007JD009551.
- Prospero, J. M., P. Ginoux, O. Torres, S. E. Nicholson, and T. E. Gill (2002), Environmental characterization of global sources of atmospheric soil dust identified with the Nimbus 7 Total Ozone Mapping Spectrometer (TOMS) absorbing aerosol product, *Rev. Geophys.*, *40*(1), 1002, doi:10.1029/2000RG000095.
- Ramanathan, V., et al. (2001), Indian Ocean Experiment: An integrated analysis of the climate forcing and effects of the great Indo-Asian haze, *J. Geophys. Res.*, *106*(D22), 28,371–28,398, doi:10.1029/2001JD900133.
- Russell, P. B., R. W. Bergstrom, Y. Shinozuka, A. D. Clarke, P. F. DeCarlo, J. L. Jimenez, M. Livingston, J. Redemann, O. Dubovik, and A. Strawa (2010), Absorption Angstrom Exponent in AERONET and related data as an indicator of aerosol composition, *Atmos. Chem. Phys.*, *10*, 1155–1169, doi:10.5194/acp-10-1155-2010.
- Streets, D. G., T. C. Bond, T. Lee, and C. Jang (2004), On the future of carbonaceous aerosol emissions, *J. Geophys. Res.*, *109*, D24212, doi:10.1029/2004JD004902.
- Torres, O., P. K. Bhartia, J. R. Herman, Z. Ahmad, and J. Gleason (1998), Derivation of aerosol properties from satellite measurements of backscattered ultraviolet radiation: Theoretical basis, *J. Geophys. Res.*, *103*(D14), 17,099–17,110, doi:10.1029/98JD00900.
- Torres, O., P. K. Bhartia, J. R. Herman, A. Sinyuk, P. Ginoux, and B. Holben (2002), A long-term record of aerosol optical depth from TOMS observations and comparison to AERONET measurements, *J. Atmos. Sci.*, *59*, 398–413.
- Torres, O., A. Tanskanen, B. Veihelmann, C. Ahn, R. Braak, P. K. Bhartia, P. Veefkind, and P. Levelt (2007), Aerosols and surface UV products from Ozone Monitoring Instrument observations: An overview, *J. Geophys. Res.*, *112*, D24S47, doi:10.1029/2007JD008809.
- Torres, O., C. Ahn, and Z. Chen (2013), Improvements to the OMI near-UV aerosol algorithm using A-train CALIOP and AIRS observations, *Atmos. Meas. Tech.*, *6*, 3257–3270, doi:10.5194/amt-6-3257-2013.
- Wagner, R., T. Ajtai, K. Kandler, K. Lieke, C. Linke, T. Müller, M. Schnaiter, and M. Vragel (2012), Complex refractive indices of Saharan dust samples at visible and near UV wavelengths: A laboratory study, *Atmos. Chem. Phys.*, *12*, 2491–2512, doi:10.5194/acp-12-2491-2012.
- Wang, J., X. Liu, S. A. Christopher, J. S. Reid, E. A. Reid, and H. Maring (2003), The effects of non-sphericity on geostationary satellite retrievals of dust aerosols, *Geophys. Res. Lett.*, *30*(24), 2293, doi:10.1029/2003GL018697.
- Yang, Z., J. Wang, C. Ichoku, E. Hyer, and J. Zeng (2013), Mesoscale modeling and satellite observation of transport and mixing of smoke and dust particles over northern sub-Saharan African region, *J. Geophys. Res. Atmos.*, *118*, 12,139–12,157, doi:10.1002/2013JD020644.